Comparison of photometer and global MHD determination of the open-closed field line boundary

I. J. Rae, K. Kabin, R. Rankin, F. R. Fenrich, and W. Liu

Department of Physics, University of Alberta, Edmonton, Alberta, Canada

J. A. Wanliss

Department of Physical Sciences, Embry-Riddle Aeronautical University, Daytona Beach, Florida, USA

A. J. Ridley, T. I. Gombosi, and D. L. De Zeeuw

Center for Space Environment Modeling, University of Michigan, Ann Arbor, Michigan, USA

[1] We compare open-closed field line boundary positions from the BATS-R-US Global MHD model and CANOPUS photometer measurements of red-line emissions. We choose intervals of steady interplanetary and ionospheric conditions in order to adhere to the "steady-state" picture that we are trying to address. Nine intervals are chosen that correspond to stable IMF and auroral conditions that can be simulated with the MHD model. We find that on average, the steady-state BATS-R-US MHD model provides an excellent estimate of the open-closed field line boundary proxy as determined by the red-line auroral emissions. Typical errors between the model calculations of the open-closed field line boundary and the observations are within the inherent error in using the red-line emissions.   *INDEX TERMS:* 2407 Ionosphere: Auroral ionosphere (2704); 2431 Ionosphere: Ionosphere/magnetosphere interactions (2736); 2753 Magnetospheric Physics: Numerical modeling; 2776 Magnetospheric Physics: Polar cap phenomena; 2740 Magnetospheric Physics: Magnetospheric configuration and dynamics; *KEYWORDS:* global MHD modeling, open-closed field line boundary, data model comparison, meridian-scanning photometer

1. Introduction

[2] The amount of energy that can be transferred between the Sun's atmosphere and the Earth's magnetosphere is highly variable. The magnetosphere stores a large amount of this energy and releases it through auroral particle precipitation and upper atmospheric heating. One way to determine how much energy is being stored in the magnetospheric system is by examining where the open/closed field line boundary (OCB) is located. The OCB is the boundary that separates magnetospheric field lines that are entangled with the sun's magnetic field lines from those that are not. Identifying the morphology of this boundary is one of the primary goals of the Geospace Environment Modeling (GEM) community [e.g., *Raeder et al.*, 1998; *Fedder et al.*, 1998]. The ability to monitor the location of the OCB allows the electrodynamics of magnetosphere-ionosphere coupling to be investigated, for example in estimating the storage and release of energy in this system during the substorm cycle [e.g., *Milan et al.*, 2003].

[3] The open/closed separatrix can be identified using particle precipitation boundaries observed by low-altitude spacecraft [*Vampola*, 1971; *Evans and Stone*, 1972]. *Vampola* [1971] showed that there is a transition between polar rain and the region of more intense, energetic particle precipitation, known as the boundary plasma sheet (BPS). *Evans and Stone* [1972] identified the "trapping boundary" as the poleward edge of high-energy (>10 keV) electron precipitation, corresponding to particles trapped on closed field lines. Field lines poleward of this region must therefore be open; however, there is still an uncertainty as to whether field lines that are only fractions of degrees equatorward of this region are also open [*Oksavik et al.*, 2000]. *Blanchard et al.* [1995] demonstrated that the poleward border of 6300Å optical emissions is very close to the transition between open and closed field lines in the dusk-midnight sector. These authors fitted a step-function in latitude to the auroral emissions and compared the boundary of these photometer emissions with low-latitude Defense Meteorological Satellite Program (DMSP) particle measurements. They found that the low-altitude "trapping boundary" was on average within ±0.9° of the poleward border of the red-line (6300Å) emissions. *Blanchard et al.* [1997] went on to assess the validity of this method by examining an entirely

different dataset of these spacecraft and photometer comparisons and found that the identification of the poleward edge of the OCB can be refined by adding a series of threshold values to the step-function criteria. They found that the average intensity of the red line emissions in the polar cap was ∼60 Rayleighs (R) and in the auroral zone ∼160 R. Taking a threshold of 110 R, they found that identifying the OCB as 0.7° equatorward of the 110 R transition, yields only a ±1.2° error in the majority of cases.

[4] In spite of its importance, it is difficult in practice to measure the global OCB for a lengthy period of time or a range of local times. Several methods distinguish this boundary via point measurements, and the use of Global Imagers is becoming increasingly important. *Elsen et al.* [1998] compared the results of a magnetohydrodynamic (MHD) model [*Winglee et al.*, 1998] with the poleward boundary of Polar Ultraviolet Imager (UVI) [*Torr et al.*, 1995] emissions for a period of ∼3.5 hours. In this study, *Elsen et al.* [1998] found that there was an average discrepancy between the Winglee model and the Polar UVI of ∼5° during the start of the interval. When the IMF became strongly southward and the magnetosphere presumably became more dynamic, the discrepancy between their observations and calculations became much larger. *Raeder et al.* [1998] presented good agreement of the separatrix from a global MHD model and the Assimilative Mapping of Ionospheric Electrodynamics (AMIE) procedure. In this paper, *Raeder et al.* [1998] simulated two time intervals that were proposed as the Geospace Environment Modeling (GEM) Grand Challenge and found that the OCBs of the MHD model and AMIE were qualitatively similar on a near-global scale during varying IMF conditions. *Slinker et al.* [2001] simulated an interval of northward IMF with a global MHD model and compared the polar cap boundary with that obtained from a meridian scanning photometer (MSP) close to the geomagnetic pole and found that the OCB in both the model and the red-line auroral emissions were in excellent agreement. However, these are isolated case studies. MSP data are routinely available, which allows the point-determination of the OCB (or polar cap boundary (PCB)). This allows us to select suitable events for comparison with a global MHD model. In this paper, we present nine case studies of steady red-line auroral emissions which occur under steady interplanetary conditions. We introduce an improved poleward border detection algorithm for the 6300Å emissions, which is based upon a Gaussian fit to the latitudinal profile of the intensity, as in the approach of *Friedrich et al.* [2001] and *Wanliss et al.* [2002]. In each case study, we compare this poleward border fit to the OCB calculated by the ''steady-state'' Block Adaptive-Tree Solar-wind Roe-type Upwind Scheme (BATS-R-US) Global MHD model [*Powell et al.*, 1999, and references therein]. We find that the point-measurements from BATS-R-US and those obtained via a Gaussian fit to the photometer measurements are in excellent agreement for the nine case studies which span ∼7 hours of local time from ∼1830–0130 MLT. Furthermore, there are very few discrepancies between the observations and the model that lie outside the inherent error defined by *Blanchard et al.* [1995, 1997]. Finally, we introduce a simple method that accounts for changes in dipole tilt angle that must be accounted for

when comparing the OCB photometer fits with the steady state BATS-R-US model.

2. BATS-R-US Model

[5] The BATS-R-US MHD code is a recently developed numerical magnetospheric model that solves the governing equations of ideal single-fluid MHD. These equations are solved on a three-dimensional unstructured adaptive grid using a Godunov-type finite volume method [*Godunov*, 1999]. The numerical details of this code are described in detail by *Powell et al.* [1999]. The model has been applied to the study of various physical phenomena, from the heliosphere to comets [e.g., *Kabin et al.*, 2000] to the Earth's magnetosphere for northward IMF conditions [e.g., *Song et al.*, 1999] and for IMF conditions corresponding to the Parker spiral angle [e.g., *Gombosi et al.*, 2000]. In the BATS-R-US model, the ionosphere is represented by a two-dimensional layer with finite Pedersen and Hall conductivities. The longitudinal and latitudinal dependencies of the Pedersen and Hall conductivities are taken from the field-aligned current particle precipitation model outlined in the work of *Ridley et al.* [2003]. The Magnetosphere-Ionosphere (M-I) coupling is obtained by using field-aligned currents in a procedure described by *Song et al.* [1999] and *Ridley et al.* [2003]. The field strength of the dipole used in BATS-R-US at the geomagnetic equator on the Earth's surface is 31100 nT.

[6] The OCB is calculated in the model via the tracing of individual field lines starting from the northern hemisphere. If a field line has footpoints in both the northern and southern ionosphere then it is obviously closed. Alternatively, a field line would be traced until it leaves the simulation box. The simulation box in our model is very large, ranging from 32 R_E upstream to 224 R_E downstream, and ±64 R_E in the Y and Z directions, so a field line usually crosses the bow shock before leaving the simulation box, at which point the field line is clearly connected to the solar wind. This procedure was applied for every magnetic latitude considered, until the transition from closed to open field lines was bracketed to ∼0.3°. We note, that 0.3° in latitude at the Earth surface is actually smaller than the grid size used in the simulations, so we used linear interpolation for the magnetic field components inside the computational cells, which is consistent with the second order solution scheme of *Powell et al.* [1999].

3. CANOPUS Photometers

[7] The Canadian Auroral Network for the Open Program Unified Study (CANOPUS) MSPs have been in operation since 1989 and are located at Rankin Inlet, Gillam, Pinawa, and Fort Smith [*Rostoker et al.*, 1995]. The photometers scan the meridian twice a minute and are integrated to 1-min resolution, and each scan is binned into 16 latitude bins. The data discussed in this paper are taken only from the Rankin Inlet (RAN) station (73.7°N, 330°E in altitude-adjusted corrected geomagnetic (AACGM) coordinates) (see *Baker and Wing* [1989] for details) as this station samples the poleward border of the auroral oval regularly. When studying auroral phenomena, data is best ordered by a coordinate system based upon the Earths magnetic field. We chose the
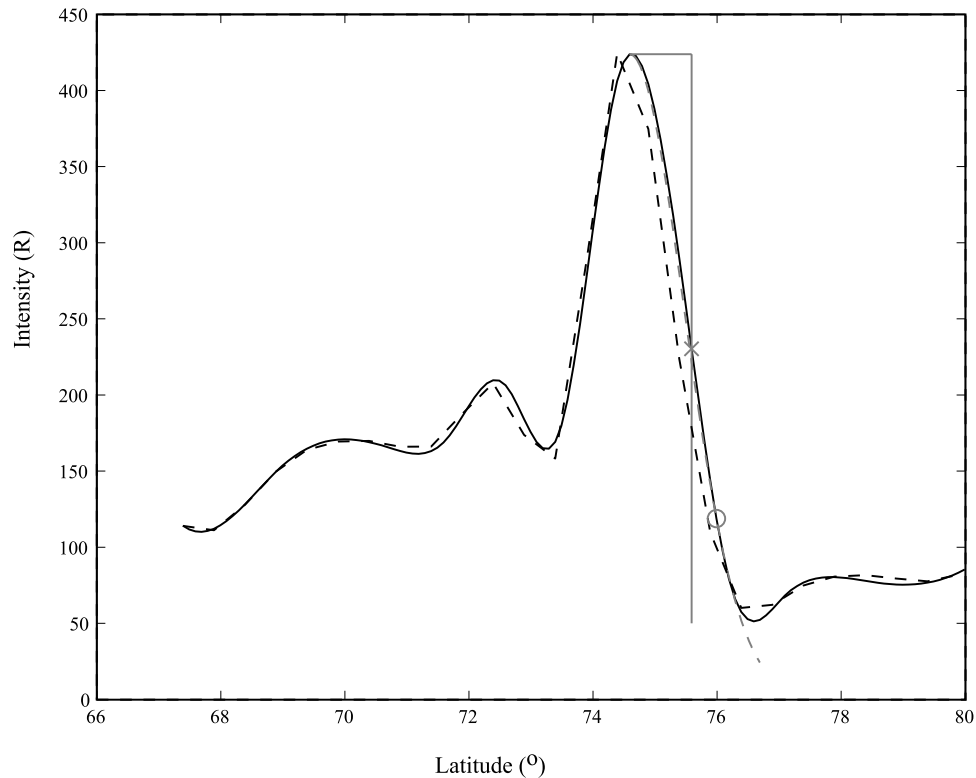
Figure 1. A latitude-intensity profile from the Rankin Inlet MSP red-line emissions, from a typical interval from this study, on 29 November 1996 0200 UT. The solid black line represents the smoothed dataset profile, the black dashed line the measured dataset, the grey dashed line represents the Gaussian fit to the curve with the difference at 1.5σ minimized and marked by the grey circle [*Friedrich et al.*, 2001]. The solid grey line represents the step-function technique employed successfully (the boundary being marked by a grey cross) in the work of *Blanchard et al.* [1995, 1997].

AACGM coordinate system as it is commonly used in the community, and the results of this study may be easily compared with previous studies of the OCB [e.g., *Slinker et al.*, 2001; *Milan et al.*, 2003].

[8] Auroral emissions in the 6300Å line may arise from a variety of mechanisms associated with low-energy (<1 keV) electron precipitation [*Blanchard et al.*, 1995]. These mechanisms are (1) chemiluminescence [*Rusch et al.*, 1978], (2) dissociative recombination of O_2^+ [*Rees and Luckey*, 1974], (3) direct excitation of atomic oxygen (to the $O(^1D)$ state) by precipitating electrons [*Rees*, 1989], and (4) cascading of excited oxygen (to the $O(^1S)$ state) through 5577Å emissions [*Rees*, 1989].

[9] Of these sources, chemiluminescence and dissociative recombination do not change as a magnetospheric or ionospheric boundary is crossed. However, emissions from direct excitation and cascading via 5577Å emissions do increase sharply equatorward of the polar cap boundary. This is primarily due to the fact that particle precipitation increases equatorward of the OCB, as does Joule heating via the ionospheric currents (see *Blanchard et al.* [1995] for a full description).

[10] In our study, we adopt the results of *Blanchard et al.* [1995] in assessing an error estimate of ±0.9° in OCB determination. The data discussed in this paper are shown in intensity and AACGM latitude versus time format, assuming that the 6300Å emissions occur at an average altitude of 230 km. The intensity can be smoothed in both latitude and time via bicubic interpolation using the 16 closest points [*Wanliss et al.*, 2002]. The smoothing reduces high gradients from the inherent data spikes and gives a smoother peak intensity profile. Fitting the precipitation boundary to the poleward border of the 6300Å emissions is based upon *Friedrich et al.* [2001]. That is, for any given UT, we fit the variation of intensity with latitude using a narrow Gaussian curve. The width of this Gaussian curve is increased until the difference between the analytical curve and the observed profile is minimised at a specific location defined by 1.5σ; where σ is the standard deviation of the Gaussian curve. This location, 1.5σ, is then taken as the poleward border. To identify the evolution of the boundary in time, this process is repeated at every time step. This method was employed in the papers of *Friedrich et al.* [2001] and *Wanliss et al.* [2002] to study the dynamics of the substorm expansive phase and magnetotail dynamics respectively. Figure 1 shows a typical latitude-intensity profile from the Rankin Inlet MSP on 29 November 1996 0200 UT. The solid black curve denotes the smoothed intensity profile at 0200 UT, the dashed black curve the measured latitudinal intensity, and the grey dashed curve represents the Gaussian curve chosen to represent this intensity profile to minimise the difference at 1.5σ (shown by the circle). For comparison, the solid grey curve shows the result of using a step function in the manner described by *Blanchard et al.* [1995], with its boundary identification

WIND MFE and SWE 961129
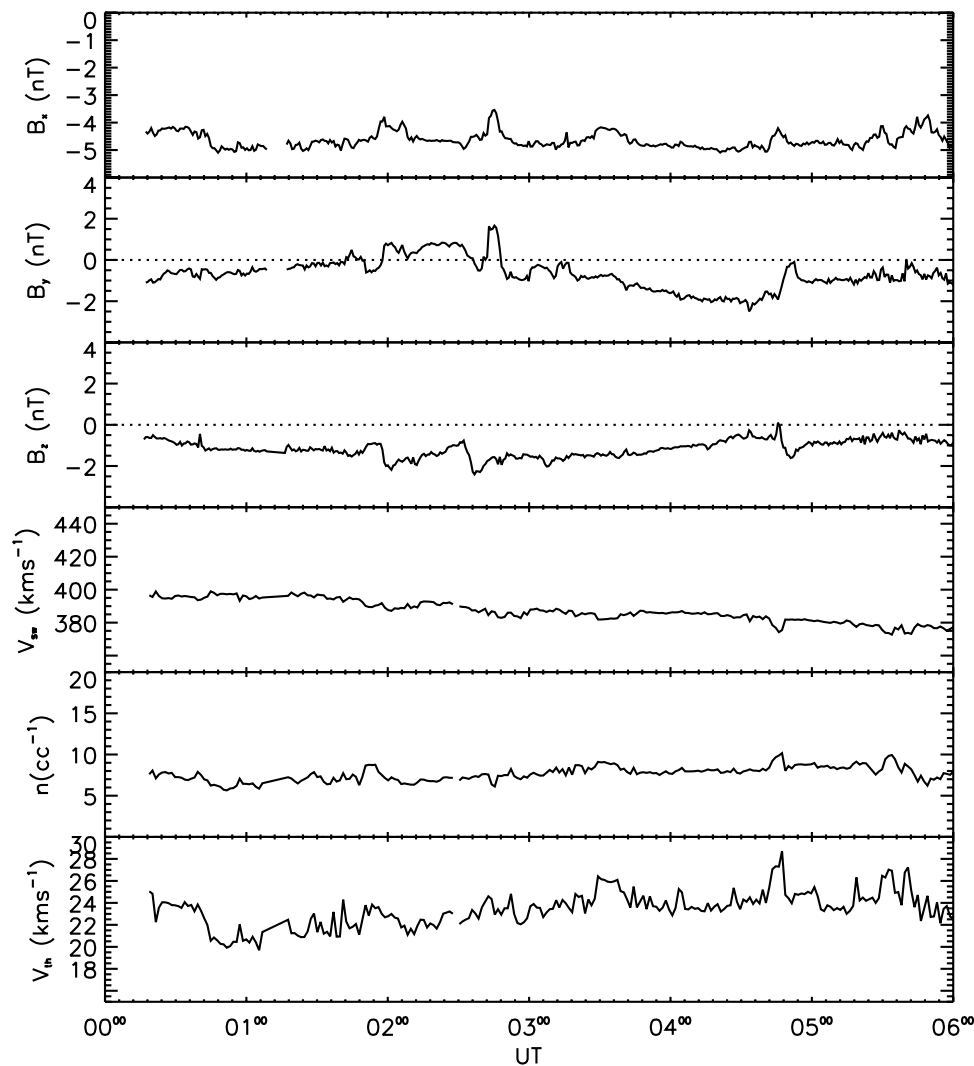
Figure 2. Solar wind and IMF conditions from the Wind spacecraft suitably lagged to the magnetopause from 29 November 1996 0000–0600 UT. Plotted from top to bottom in Figure 2 is IMF B_x, B_y, B_z (in GSM coordinates) solar wind velocity (V_{sw}), proton number density (n) and thermal velocity (V_{th}).

shown as a grey cross. It must be stressed that these smooth intensity profiles are not typically observed in the 6300Å emission line. These case studies have been chosen to adhere to the criteria outlined below, and are thus a very unusual dataset.

4. Event Criteria

[11] The events selected for this "steady-state" study were specifically selected to resemble periods where the near-Earth environment could be approximated by the steady-state solution of BATS-R-US. In order for this condition to be upheld we selected intervals that satisfied the following conditions:

[12] 1. Periods of steady auroral emissions at the Rankin Inlet station for over 2 hours. In these cases, "steady" was defined by the requirement that the poleward boundary did not vary over more than 4° during the interval.

[13] 2. Little ground magnetic activity observed in the magnetometers along the Churchill line of the CANOPUS magnetometer network on which Rankin Inlet MSP is located, i.e., no evidence of substorm activity.

[14] 3. During each interval, the available solar wind monitor(s) recorded relatively constant or slowly varying IMF and solar wind conditions.

[15] With steady interplanetary conditions and steady auroral conditions in the ionosphere, there is the expectation that "steady-state" principles will hold true. This is important for several reasons: Due to the computationally intensive nature of the BATS-R-US MHD model, it is unrealistic to run a very large number of cases to verify the boundary identifications in the model. We therefore selected nine intervals under the most stable IMF and auroral conditions. These nine intervals occur in the winter hemisphere, when the MSPs run for the long periods of time. In principle, we see no reason why these results would not also translate into

Table 1. A Summary of the Observed and Simulated Intervals Incorporated in This Study[a]

Date	UT	MLT	Φ	B_x	B_y	B_z	V_{sw}	N	V_{th}	θ_{RAN}	θ_{BRU}	$d\theta$
961129	0100	1816	−27.5	−4	−1	−1.2	−395	6.5	22	76.0	77.0	−1.0
	0130	1846	−28.6	−4	−1	−1.2	−395	6.5	22	74.7	76.6	−1.9
	0200	1916	−29.6	−4	−1	−1.2	−395	6.5	22	75.9	76.0	−0.1
	0230	1946	−30.5	−4	−1	−1.2	−395	6.5	22	76.2	75.4	0.8
	0300	2016	−31.2	−4	−1	−1.2	−395	6.5	22	75.2	74.9	0.3
960314	0300	2016	−11.8	−2	−3	−2	−560	2.7	45	73.5	72.6	0.9
	0330	2046	−12.3	−2	−3	−2	−560	2.7	45	73.2	72.3	0.9
	0400	2116	−12.8	−2	−3	−2	−560	2.7	45	72.6	71.8	0.8
	0430	2146	−13.0	−2	−3	−2	−560	2.7	45	72.6	71.8	0.8
	0500	2216	−13.1	−2	−3	−2	−560	2.7	45	74.8	71.8	3.0
971218	0200	1916	−31.2	3	−5	−6	−300	17	20	72.0	73.8	−1.8
	0230	1946	−32.0	3	−5	−6	−300	17	20	72.4	73.3	−0.9
	0300	2016	−32.8	3	−5	−6	−300	17	20	72.3	72.8	−0.5
	0330	2046	−33.4	3	−5	−6	−300	17	20	70.4	72.2	−1.8
	0400	2116	−33.7	3	−5	−6	−300	17	20	71.2	72.0	−0.8
950224	0500	2216	−20.3	1.7	2	0	−305	18	19	72.0	71.1	0.9
	0530	2246	−20.2	1.7	2	0	−305	18	19	72.1	71.2	0.9
	0600	2316	−19.9	1.7	2	0	−305	18	19	72.1	71.2	0.9
	0630	2346	−19.4	1.7	2	0	−305	18	19	73.3	71.3	2.0
	0700	0016	−18.8	1.7	2	0	−305	18	19	73.3	71.3	2.0
950306	0600	2316	−14.5	4	2.5	6	−460	8	50	73.8	72.5	1.3
	0630	2346	−14.5	4	2.5	6	−460	8	50	73.1	72.4	0.7
	0700	0016	−14.5	4	2.5	6	−460	8	50	72.7	72.7	0.0
	0718	0034	−14.5	4	2.5	6	−460	8	50	72.9	73.2	−0.3
	0730	0046	−14.5	4	2.5	6	−460	8	50	73.8	73.2	0.6
	0800	0116	−14.5	4	2.5	6	−460	8	50	75.1	72.3	2.8
950209	0349	2105	−25	5	7	−0.5	−412	7	26	72.9	72.3	−0.4
950223	0542	2258	−20.5	2	5	−2	−310	10	25	71.5	71.5	0.0
950226	0315	2031	−18.5	2	6.5	−2	−270	28	22	74.8	71.2	3.6
961216	0515	2231	−33.8	−4	−2	−1	−550	5.5	55	70.6	72.2	−1.6

[a]Included in Table 1 are the UT, MLT, dipole tilt (Φ), prevailing IMF and solar wind plasma conditions, observed photometer open-closed field line boundary (θ_{RAN}), BATS-R-US simulated open-closed field line boundary (θ_{BRU}), and the difference between them ($d\theta$).

the summer hemisphere. However, in this study we found no intervals that satisfied all of our criteria in the summer hemisphere.

5. Solar Wind Conditions

[16] Figure 2 shows the solar wind and interplanetary conditions from the first simulated interval on 29 November 1996 0000−0600 UT, suitably lagged to the magnetopause, as determined from the Wind spacecraft. From the top, in descending order, is IMF B_x, B_y, B_z, solar wind speed V_{sw}, proton number density n_{sw}, and thermal velocity v_{th} in GSM coordinates. Figure 2 shows that the lagged solar wind conditions are very steady over a long interval, for most of the 6-hour interval. In this case study, B_x was ∼−5 nT, B_y was ∼−1 nT (though it did have an interval of weakly positive B_y between 0200 and 0300 UT) and B_z was ∼−1 nT. The solar wind speed (V_{sw}) was relatively steady between ∼380 and 400 kms^{-1}, proton number densities (n) between 7 and 8 cc^{-1}, and thermal speeds (V_{th}) of 20−26 kms^{-1}. The nine events were under similarly constant but very different solar wind and IMF conditions (see Table 1). During these nine intervals, IMF B_x ranges from −4nT to +5nT, IMF B_y ranges from −5 to +7 nT, and IMF B_z from −6 nT to +6 nT. Solar wind number density ranges from 2.7 to 28 cc^{-1}, solar wind V_x ranges between −560 and −270 kms^{-1}, and thermal velocities range between 19 and 55 kms^{-1}. We found only one case study under positive IMF B_z conditions and one of near-zero IMF B_z given our selection criteria. In the case study shown in Figure 2, we chose 0100 UT as the starting point for the simulation, and we assume that the starting conditions can

approximate the entire interval of interest, in this case, 0100−0300 UT. Table 1 summarizes all the relevant data from these case studies, including the prevailing IMF and solar wind plasma conditions prevalent during them.

6. Comparison of Photometer and Simulation Results

[17] Figure 3 shows 2 hours of photometer data from five of the days at Rankin Inlet (RAN) in latitude-time-intensity format (from 10^2 to 10^3 Rayleighs) that were simulated with the BATS-R-US code. The days and start times of the intervals shown are (a) 961129 0100 UT, (b) 971218 0200 UT, (c) 960314 0300 UT, (d) 950224 0500 UT, and (e) 950306 0600 UT. Overplotted on each of the panels in Figure 3 is the identification of the poleward border of the redline emissions, outlined in section 3, and shown by the white lines. The black and white crosses denote the times where the BATS-R-US model was run to a steady-state solution, and the open-closed field line boundary at the local time of the photometer was either extracted or calculated. For example, in Figures 3a and 3b, we ran the BATS-R-US model to steady-state solution at 0100 UT and 0300 UT respectively, and, assuming the same solar wind conditions (i.e., steady-state conditions), altered the Earth's dipole tilt angle to the appropriate value every 30 min and ran the model to steady state again. Thus, the series of crosses in Figures 3a and 3b show the effect of changing dipole tilt and local time, in the BATS-R-US model. However, for the ensuing three intervals shown in Figure 3, we used an approximate procedure to define the OCB at different UTs. Indeed if the solar wind parameters do not change during an
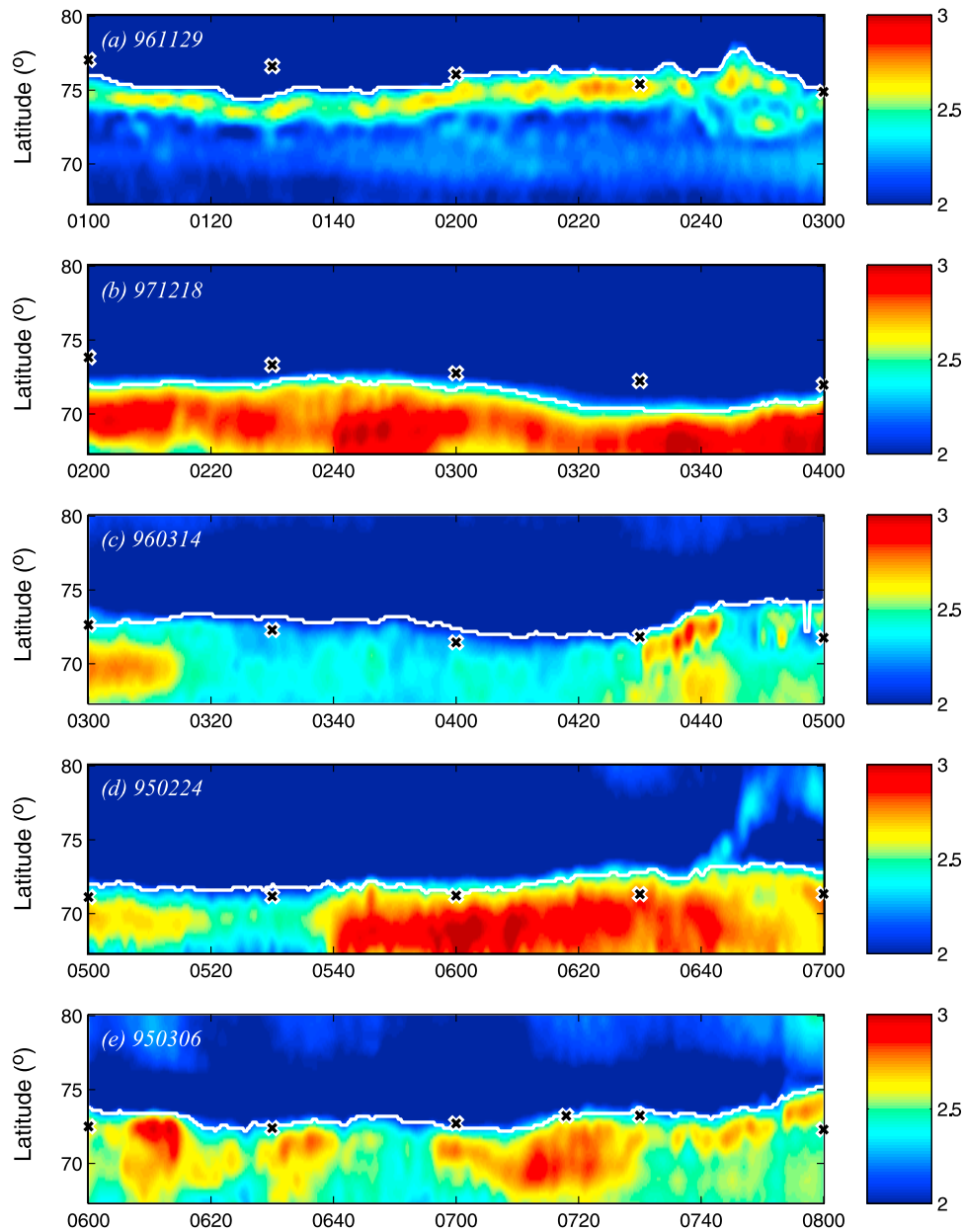
Figure 3. Five latitude-time-intensity plots of photometer data from the Rankin Inlet (RAN) meridian scanning photometer. These intervals were simulated in steady-state mode with the BATS-R-US MHD model. The days and start times of the intervals shown are (a) 961129 0100 UT, (b) 960314 0300 UT, (c) 971218 0200 UT, (d) 950224 0500 UT, and (e) 950306 0600 UT. Overplotted on each of the figures is the identification of the poleward border of the red-line emissions shown by the white lines. The black and white crosses denote the times where the BATS-R-US model was run to a steady-state solution, and the open-closed field line boundary at the local time of the photometer was extracted.

interval, then the only input variable into the BATS-R-US model that changes is dipole tilt angle (in GSM coordinates). Furthermore, the intervals in this paper are 2 hours long, and during these intervals the dipole tilt angle changes by less than 5°. Therefore instead of rerunning BATS-R-US at each time point, we attempt to simplify the procedure by extrapolating the OCB obtained for a specific dipole tilt, Φ, to other angles that are close to the initial value of Φ.

[18] Specifically, we start with an OCB at a particular UT corresponding to a particular Φ. Then we rotate the OCB by the change in Φ corresponding to a different UT in GSM coordinates and transform the results into AACGM coordinates at the new UT. To illustrate this, we used the results obtained in the 29 November 1996 interval (shown in Figure 3a), for which there were five instances simulated. Figure 4 shows the polar cap boundaries looking down on the northern hemispheric ionosphere with local noon at the top of the page. The OCB calculated at 0100 UT (black line) and 0300 UT (grey line) are shown over the entire polar cap. The grey circles denote the result obtained by
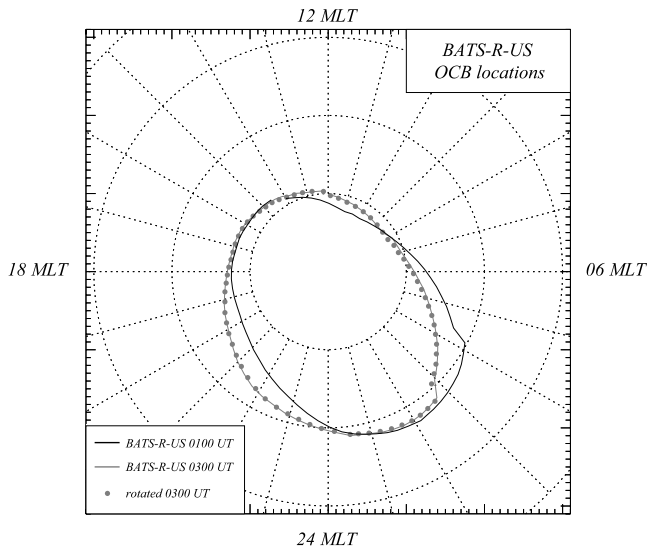
Figure 4. The results of running the BATS-R-US model to a "steady-state" solution of 29 November 1996 shown as a polar plot looking down on the northern hemispheric ionosphere in AACGM co-ordinates with local noon at the top of the page. Dotted circles represent 60°, 70°, and 80° MLAT, and radial lines represent MLT meridians. Also shown in Figure 4 are the simulated results run with appropriate dipole tilt angles at 0100 UT (black line) and 0300 UT (grey line). Overplotted in grey circles is the result of using the polar cap boundary at 0100 UT and rotating it by the change in dipole tilt between the two times. The difference in using this technique is negligible.

taking the polar cap boundary at 0100 UT and simply rotating it by the appropriate change in dipole tilt between 0100 and 0300 UT (−3.7° in GSM coordinates). From Figure 4, we can see that the difference in rerunning BATS-R-US and rotating the solution by an appropriate dipole tilt change is negligible. The same result was found for the event shown in Figure 3b which was run an hour either side of the initial time that the model was run. These results give fortitude to our assumptions that it is possible to obtain the steady-state solution at any given point in a steady-state interval and rotate the calculated OCB by the appropriate change in dipole tilt to obtain the OCB at a new time. Thus for the ensuing three intervals shown in Figure 3, the BATS-R-US "steady-state" solutions were obtained at (c) 0300 UT, (d) 0500 UT, and (e) 0718 UT, and to obtain the boundary at different UTs (and therefore MLTs), the polar cap boundary was rotated by the change in dipole tilt.

[19] The mean latitude of the boundary of red line emissions in Figure 3a (961129) is 75.6° ± 2.0°, where 2.0° is the maximum variation during the 2 hour interval. The average BATS-R-US boundary is 76.0°, so the average difference is ∼−0.4°. That is, the BATS-R-US boundary is on average 0.4° poleward of the boundary of the emissions. During the interval on 971218 (Figure 3b), the BATS-R-US boundary is always poleward of the OCB identified by the auroral emissions. The mean latitude of the boundary identified by the auroral emissions is 71.6° ± 1.3°, the average BATS-R-US boundary is 72.8°, so the average difference between the two boundary identifications is

**Table 2.** A Summary of the Average Values and Variations Between the MSP Determined OCB and the BATS-R-US Boundary[a]

Event	Av. θ_{MSP} (°)	Max Variation (°)	Av. θ_{BRU} (°)	Av. dθ
961129	75.6	2.0	76.0	−0.4
971218	71.6	1.3	72.8	−1.2
960314	73.3	1.4	72.0	1.3
950224	72.6	1.2	71.2	1.4
950306	73.6	2.0	72.7	0.9

[a]Included in Table 2 is the average MSP boundary (Av. θ_{MSP}), maximum variation in the MSP boundary within the interval, average BATS-R-US boundary (Av. θ_{BRU}) and the average difference between the boundary identifications (dθ).

−1.2°. Conversely, during the comparison on 960314 (Figure 3c), the BATS-R-US boundary is equatorward of the red-line emission boundary for the interval. The average latitude of the red-line boundary is 73.3° ± 1.4°. The average boundary obtained from the MHD model is ∼72.0° and the average difference between the boundaries is 1.3°. The case study of 950224 (Figure 3d) again sees the BATS-R-US boundary equatorward of the 6300Å emission boundary. The average 6300Å boundary latitude is 72.6° ± 1.2°, the average BATS-R-US boundary latitude is 71.2°, and the average difference is 1.4°. Finally, Figure 3e shows the case study on 950306 0600−0800 UT. The average latitude of the photometer boundary is 73.6° ± 2.0°, the average boundary extracted from the MHD model is 72.7°, and the average difference is 0.9°. These comparisons are summarized in Table 2.

[20] These time-point comparisons can also be shown in magnetic latitude: magnetic local time format (MLT: MLAT). Figure 5 shows the colour-coded comparisons of
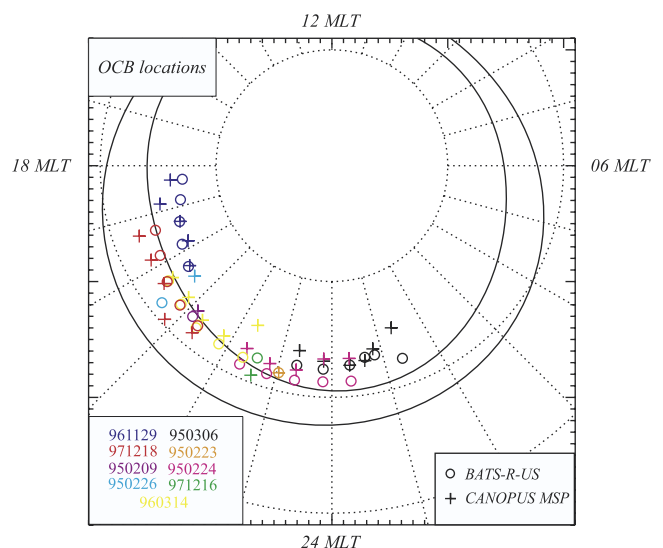
Figure 5. A magnetic local time: magnetic latitude (MLT: MLAT) plot of the ionospheric projection of the OCBs in the same format as Figure 4. Crosses denote the observed OCB points, and circles denote the BATS-R-US calculated OCBs. Each observed point has a corresponding simulated point, and each simulated interval is denoted by a color code (see key in Figure 5). The solid lines denote an average position of the auroral oval for Kp = 2.

the OCB obtained via a fit to the RAN 6300Å emissions (crosses) and the BATS-R-US calculated values (circles) in the same format as Figure 4. These results cover over 7 hours of MLT, and the maximum variation is $\sim 3.6°$. On average, the simulated open-closed field line boundary is $0.4°$ equatorward of the photometer boundary.

[21] The case studies we have presented take place over a large range of IMF conditions, though we have not found more than one case study under northward IMF. We hope to address this point in future. However, it is encouraging to find that the $1.4°$ rms deviation between the measured and simulated OCBs is comparable to the inherent errors introduced by using the 6300Å as an OCB proxy. Under steady auroral conditions the magnetosphere can be approximated by steady-state conditions. Under steady IMF/solar wind conditions the solar-wind magnetospheric interaction can also be approximated by steady state. In these cases we show that the BATS-R-US model can reproduce this important set of observations.

7. Discussion and Conclusions

[22] We present a nine-event comparison of the ionospheric proxy of the open-closed field line boundary (as determined by Rankin Inlet MSP measurements) with steady-state solutions of the OCB calculated from the BATS-R-US Global MHD model. These nine events occurred under steady but substantially different solar wind and IMF conditions. Events were selected on the basis that there should be no significant transient activity (i.e., steady auroral conditions). These events typically occurred in the dusk sector ionosphere and covered a wide range of local times in the dusk-midnight sector. During such intervals, we find excellent agreement between the OCB defined by the photometer observations and the BATS-R-US OCB calculations. Furthermore, we show that under steady state conditions, the OCB variation due to dipole tilt changes can be approximated by simply rotating the OCB by the increment of the dipole tilt angle (in GSM coordinates). During intervals that we have simulated, the dipole tilt variation was typically of the order of $3°$, and so we have established that our methodology is valid for dipole changes of at least this magnitude. In this way, the run time of the model is reduced, and hence the applicability of BATS-R-US to further and future studies is improved. The excellent comparisons support the use of BATS-R-US to model slowly varying phenomena, with one potential application being to use the BATS-R-US OCB boundary location as a monitor of energy storage during the growth phase of magnetic substorms.

[23] We have found that the average discrepancy between the BATS-R-US model and the observed OCBs is $0.4°$ with $\sigma = 1.4°$ which means that the photometer boundary is on average $0.4°$ poleward of the BATS-R-US boundary; hence the BATS-R-US model boundary shows excellent agreement with the ionospheric OCB proxy. There were also individual discrepancies as large as $-1.9°$ (BATS-R-US poleward of MSP boundary) and $3.6°$ (MSP poleward of BATS-R-US), though these were rare. The largest discrepancies occurred towards the end of the intervals and may be due to the fact that the steady-state approximation may no longer hold true for a few of the chosen intervals. The data/

model comparison can also be split into MLT sector. Between 1800 and 2100 MLT, it was found that on average the BATS-R-US boundary position measurements lay slightly poleward of the auroral emission boundaries, whereas this situation was reversed between 2100 and 0130 MLT. It is not clear why this occurs, and in future studies we will compare the BATS-R-US observations with observational data on a more global scale. Steady-state analysis is still vital as a validation of our methodology and is necessary before we can proceed to the study of OCB dynamics on a global scale. In this study we show that an MHD approach may easily represent the OCB when the magnetosphere is in quasi "steady state."

References

Baker, K. B., and S. Wing (1989), A new magnetic coordinate system for conjugate studies at high-latitudes, *J. Geophys. Res.*, *94*, 9139.

Blanchard, G. T., L. R. Lyons, J. C. Samson, and F. J. Rich (1995), Locating the polar cap boundary from observations of 6300 Å emission, *J. Geophys. Res.*, *100*, 7855.

Blanchard, G. T., L. R. Lyons, and J. C. Samson (1997), Accuracy of using the 6300Å auroral emission to identify the magnetic separatrix on the nightside of the Earth, *J. Geophys. Res.*, *102*, 9697.

Elsen, R. K., R. M. Winglee, J. F. Spann, G. A. Germany, M. Brittnacher, and G. K. Parks (1998), The auroral oval boundaries on January 10, 1997: A comparison of global magnetospheric simulations with UVI images, *Geophys. Res. Lett.*, *25*, 2585.

Evans, L. C., and E. C. Stone (1972), Electron polar cap and the boundary of open geomagnetic fieldlines, *J. Geophys. Res.*, *77*, 5580.

Fedder, J. A., S. P. Slinker, and J. G. Lyon (1998), A comparison of global numerical simulation results to data for the January 27–28, 1992, Geospace Environment Modeling challenge event, *J. Geophys. Res.*, *103*, 14,799.

Friedrich, E., J. C. Samson, I. Voronkov, and G. Rostoker (2001), Dynamics of the substorm expansive phase, *J. Geophys. Res.*, *106*, 13,145.

Godunov, S. K. (1999), Reminiscences about different schemes, *J. Comput. Phys.*, *153*, 6.

Gombosi, T., D. L. DeZeeuw, C. P. T. Groth, and K. G. Powell (2000), Magnetospheric configuration for Parker-spiral IMF conditions: Results of a 3D AMR MHD simulation, *Adv. Space. Res.*, *26*, 139.

Kabin, K., K. C. Hansen, T. I. Gombosi, M. R. Combi, T. J. Linde, D. L. De Zeeuw, C. P. T. Groth, K. G. Powell, and A. F. Nagy (2000), Global MHD simulations of space plasma environments: Heliosphere, comets, magnetospheres of planets and satellites, *Astron. Space. Sci.*, *274*, 407.

Milan, S. E., M. Lester, S. W. H. Cowley, K. Oksavik, M. Brittnacher, R. A. Greenwald, G. J. Sofko, and J.-P. Villain (2003), Variations in polar cap area during two substorm cycles, *Ann. Geophys.*, *21*, 1121.

Oksavik, K., F. Søraas, J. Moen, and W. J. Burke (2000), Optical and particle signatures of magnetospheric boundary layers near magnetic noon: Satellite and ground-based observations, *J. Geophys. Res.*, *105*, 27,555.

Powell, K. G., P. L. Roe, T. J. Linde, T. I. Gombosi, and D. L. De Zeeuw (1999), A solution-adaptive upwind scheme for Ideal magnetohydrodynamics, *J. Comput. Phys.*, *154*, 284.

Raeder, J., J. Berchem, and M. Ashour-Abdalla (1998), The Geospace Environment Modeling Grand Challenge: Results from a global geospace circulation model, *J. Geophys. Res.*, *103*, 14,787.

Rees, M. H. (1989), *Physics and Chemistry of the Upper Atmosphere*, Cambridge Univ. Press, New York.

Rees, M. H., and D. Luckey (1974), Auroral emission energy derived from ratios of spectroscopic emissions: 1. Model computations, *J. Geophys. Res.*, *79*, 5181.

Ridley, A. J., T. I. Gombosi, and D. L. De Zeeuw (2003), Ionospheric control of the magnetospheric configuration (1): Conductance, *Ann. Geophys.*, in press.

Rostoker, G., J. C. Samson, F. Creutzberg, T. J. Hughes, D. R. McDiarmid, A. G. McNamara, A. Vallance Jones, D. D. Wallis, and L. L. Cogger (1995), CANOPUS—A ground-based instrument array for remote sensing the high latitude ionosphere during the ISTP/GGS program, *Space Sci. Rev.*, *71*, 743.

Rusch, D. W., J. C. Gérard, and W. E. Sharp (1978), The reaction of $N(^2D)$ with O_2 as a source of $O(^1D)$ atoms in the aurorae, *Geophys. Res. Lett.*, *5*, 1043.

Slinker, S. P., J. A. Fedder, D. J. McEwen, Y. Zhang, and J. G. Lyon (2001), Polar cap study during northward interplanetary magnetic field on 19 January 1998, *Phys. Plasmas*, *8*, 1119.

Song, P., D. L. DeZeeuw, T. I. Gombosi, C. P. T. Groth, and K. G. Powell (1999), A numerical study of solar wind-magnetosphere interaction for northward interplanetary magnetic field, *J. Geophys. Res.*, *104*, 28,361.

Torr, M. R., et al. (1995), A far ultraviolet imager for the International Solar- Terrestrial Physics mission, *Space Sci. Rev.*, *71*, 329.

Vampola, A. L. (1971), Access of solar electrons to closed field lines, *J. Geophys. Res.*, *76*, 36.

Wanliss J. A., R. Rankin, J. C. Samson, and V. T. Tikhonchuk (2002), Field line resonances in a stretched magnetotail: CANOPUS optical and magnetometer observations, *J. Geophys. Res.*, *107*(A7), 1029, doi:10.1029/2001JA000257.

Winglee, R. M., S. Kokubun, R. P. Lin, and R. P. Lepping (1998), Flux rope structures in the magnetotail: Comparison between Wind/Geotail observations and global simulations, *J. Geophys. Res.*, *103*, 135.

———————————

D. L. De Zeeuw, T. I. Gombosi, and A. J. Ridley, Center for Space Environment Modeling, University of Michigan, Ann Arbor, MI 48109, USA. (darrens@engin.umich.edu; tamas@umich.edu; ridley@umich.edu)

F. R. Fenrich, K. Kabin, W. Liu, R. Rankin, and I. J. Rae, Department of Physics, University of Alberta, Edmonton, Alberta T6G 2J1, Canada. (frances@space.ualberta.ca; kabin@space.ualberta.ca; wliu@space.ualberta.ca; rankin@space.ualberta.edu; jrae@phys.ualberta.ca)

J. A. Wanliss, Department of Physical Sciences, Embry-Riddle Aeronautical University, Daytona Beach, FL 32114, USA. (wanlib01@erau.edu)